Hybrid gap modes induced by fiber taper waveguides: application in spectroscopy of single solid-state emitters deposited on thin films.

Marcelo Davanço[*1,2] **and Kartik Srinivasan**[1]

[1]*Center for Nanoscale Science and Technology, National Institute of Standards and Technology, Gaithersburg, MD*
[2]*Maryland NanoCenter, University of Maryland, College Park, MD, 20742*
[*]*Corresponding author: mdavanco@nist.gov*

Abstract: We show, via simulations, that an optical fiber taper waveguide can be an efficient tool for photoluminescence and resonant, extinction spectroscopy of single emitters, such as molecules or colloidal quantum dots, deposited on the surface of a thin dielectric membrane. Placed over a high refractive index membrane, a tapered fiber waveguide induces the formation of hybrid mode waves, akin to dielectric slotted waveguide modes, that provide strong field confinement in the low index gap region. The availability of such gap-confined waves yields potentially high spontaneous emission enhancement factors (≈ 20), fluorescence collection efficiencies (≈ 23 %), and transmission extinction (≈ 20 %) levels. A factor of two improvement in fluorescence and extinction levels is predicted if the membrane is instead replaced with a suspended channel waveguide. Two configurations, for operation in the visible (≈ 600 nm) and near-infrared (≈ 1300 nm) spectral ranges are evaluated, presenting similar performances.

References and links

1. V. R. Almeida, Q. Xu, C. A. Barrios, and M. Lipson, "Guiding and confining light in void nanostructure," Opt. Lett. **29**, 1209–1211 (2004).
2. A. H. J. Yang, S. D. Moore, B. S. Schmidt, M. Klug, M. Lipson, and D. Erickson, "Optical manipulation of nanoparticles and biomolecules in sub-wavelength slot waveguides," Nature **457**, 71–75 (2009).

3. C. Koos, P. Vorreau, T. Vallaitis, P. Dumon, W. Bogaerts, R. Baets, B. Esembeson, I. Biaggio, T. Michinobu, F. Diederich, W. Freude, and J. Leuthold, "All-optical high-speed signal processing with silicon-organic hybrid slot waveguides," Nat. Photon. **3**, 216–219 (2009).
4. Y. C. Jun, R. M. Briggs, H. A. Atwater, and M. L. Brongersma, "Broadband enhancement of light emission insilicon slot waveguides," Opt. Express **17**, 7479–7490 (2009). http://www.opticsexpress.org/abstract.cfm?URI=oe-17-9-7479
5. W. Moerner, "Examining nanoenvironments in solids on the scale of a single, isolated inpurity molecule," Science **265**, 46–53 (1994).
6. W. E. Moerner, "Single-photon sources based on single molecules in solids," New Journal of Physics **6**, 88 (2004).
7. J. Hwang, M. Pototschnig, R. Lettow, G. Zumofen, A. Renn, S. Gotzinger, and V. Sandoghdar, "A single-molecule optical transistor," Nature **460**, 76–80 (2009).
8. K. Srinivasan, O. Painter, A. Stintz, and S. Krishna, "Single quantum dot spectroscopy using a fiber taper waveguide near-field optic," Appl. Phys. Lett. **91**, 091 102 (2007).
9. M. Davanço and K. Srinivasan, "Efficient spectroscopy of single embedded emitters using optical fiber taper waveguides," Opt. Express **17**, 10 542–10 563 (2009).
10. M. Davanço and K. Srinivasan, "Fiber-coupled semiconductor waveguides as an efficient optical interface to a single quantum dipole," Opt. Lett. **34**, 2542–2544 (2009). http://ol.osa.org/abstract.cfm?URI=ol-34-16-2542
11. A. W. Snyder and J. D. Love, *Optical Waveguide Theory* (Chapman and Hall, New York, NY, 1983).
12. I. Gerhardt, G. Wrigge, P. Bushev, G. Zumofen, M. Agio, R. Pfab, and V. Sandoghdar, "Strong Extinction of a Laser Beam by a Single Molecule," Phys. Rev. Lett. **98**, 033 601 (2007).
13. J. Lee, V. C. Sundar, J. R. Heine, M. G. Bawendi, and K. F. Jensen, "Full Color Emission from II-VI Semiconductor Quantum Dot-Polymer Composites," Adv. Mater. **12**, 1102–1105 (2000).
14. R. D. Schaller, M. A. Petruska, and V. Klimov, "Tunable Near-Infrared Optical Gain and Amplified Spontaneous Emission Using PbSe Nanocrystals," J. Phys. Chem. B **107**, 13 765–13 768 (2003).
15. A. Zumbusch, L. Fleury, R. Brown, J. Bernard, and M. Orrit, "Probing individual two-level systems in a polymer by correlation of single molecule fluorescence," Phys. Rev. Lett. **70**, 3584–3587 (1993).
16. M. Orrit and J. Bernard, "Single pentacene molecules detected by fluorescence excitation in a p-terphenyl crystal," Phys. Rev. Lett. **65**, 2716–2719 (1990).
17. G. S. Harms, T. Irngartinger, D. Reiss, A. Renn, and U. P. Wild, "Fluorescence lifetimes of terrylene in solid matrices," Chemical Physics Letters **313**, 533 – 538 (1999).
18. T. Böttger, C. W. Thiel, Y. Sun, and R. L. Cone, "Optical decoherence and spectral diffusion at 1.5 μ in Er^{3+}:Y_2SiO_5 versus magnetic field, temperature, and Er^{3+} concentration," Physical Review B (Condensed Matter and Materials Physics) **73**, 075 101 (2006).
19. W.-P. Huang, "Coupled-mode theory for optical waveguides: and overview," J. Opt. Soc. Am. A **11**, 963–983 (1994).
20. Following Ref.[19], the fiber mode fraction, Eq.(2), would be given by the expression $f_m = \langle f|m\rangle\langle m|f\rangle \left(\langle f|f\rangle\langle m|m\rangle\right)^{-1}$, where $\langle f|m\rangle = \iint \left(\mathbf{e}_f \times \mathbf{h}_m^* + \mathbf{h}_f \times \mathbf{e}_m^*\right)\cdot\hat{z}\,dS/4$. Considering no reflections at the interface between the isolated fiber and the contact region, (i.e., the field just after the interface is identical to the incident, foward propagating, field), Eq.(2) gives the same result.
21. S. J. van Enk, "Atoms, dipole waves, and strongly focused light beams," Phys. Rev. A **69**,

043 813 (2004).
22. F. Wise, "Lead salt quantum dots: The limit of strong quantum confinement," Acc. Chem. Res. **33**, 773–780 (2000).
23. R. J. Pfab, J. Zimmermann, C. Hettich, I. Gerhardt, A. Renn, and V. Sandoghdar, "Aligned terrylene molecules in a spin-coated ultrathin crystalline film of p-terphenyl," Chemical Physics Letters **387**, 490 – 495 (2004).
24. V. S. C. M. Rao and S. Hughes, "Single quantum-dot Purcell factor and beta factor in a photonic crystal waveguide," Phys. Rev. B **75**, 205 437 (2007).
25. G. Lecamp, P. Lalanne, and J. P. Hugonin, "Very Large Spontaneous-Emission beta Factors in Photonic-Crystal Waveguides," Phys. Rev. Lett. **99** (2007).
26. G. Wrigge, I. Gerhardt, J. Hwang, G. Zumofen, and V. Sandoghdar, "Efficient coupling of photons to a single molecule and the observation of its resonance fluorescence," Nature Physics **4**, 60–66 (2008).
27. M. T. Rakher, R. Bose, C. W. Wong, and K. Srinivasan, "Spectroscopy of 1.55 μm PbS Quantum Dots on Si Photonic Crystal Cavities with a Fiber Taper Waveguide," arXiv:0912.1365v1 (2009).
28. M. W. McCutcheon and M. Loncar, "Design of a silicon nitride photonic crystal nanocavity with a Quality factor of one million for coupling to a diamond nanocrystal," Opt. Express **16**, 19 136–19 145 (2008).
http://www.opticsexpress.org/abstract.cfm?URI=oe-16-23-19136
29. R. F. Oulton, V. J. Sorger, T. Zentgraf, R.-M. Ma, C. Gladden, L. Dai, G. Bartal, and X. Zhang, "Plasmon lasers at deep subwavelength scale," Nature **461**, 629–632 (2009).

1. Introduction

In Ref. [1], a dielectric waveguide structure, consisting of two high refractive index regions separated by a narrow, low refractive index slot, was shown to support propagating modes with a very high field concentration in the slot region. The strong field confinement was shown to be related to the continuity of the electric displacement vector component across the gap, and to increase with index contrast. The availability of such modes offers numerous possibilities for the realization of integrated optical devices that exploit spatial localization [2], enhanced nonlinearities [3], and field-matter interaction [4] within the gap region.

In this paper, we use electromagnetic simulations to show that an optical fiber taper waveguide (sometimes called a micro- or nanofiber waveguide) can be used as an efficient probe for resonant and non-resonant spectroscopy of individual emitters bound to the surface of thin dielectric membranes. High probing efficiency is possible due to the availability of hybrid guided waves akin to the air-slot waveguide modes introduced in [1]. Such hybrid waves, referred to as gap modes, display strong field concentration in the gap between fiber and membrane and at the same time couple efficiently to the access optical fiber waveguide mode. The first feature leads to spontaneous emission rate enhancement, while the second, combined with high percentage coupling of spontaneous emission into gap modes, leads to high fluorescence collection ef-

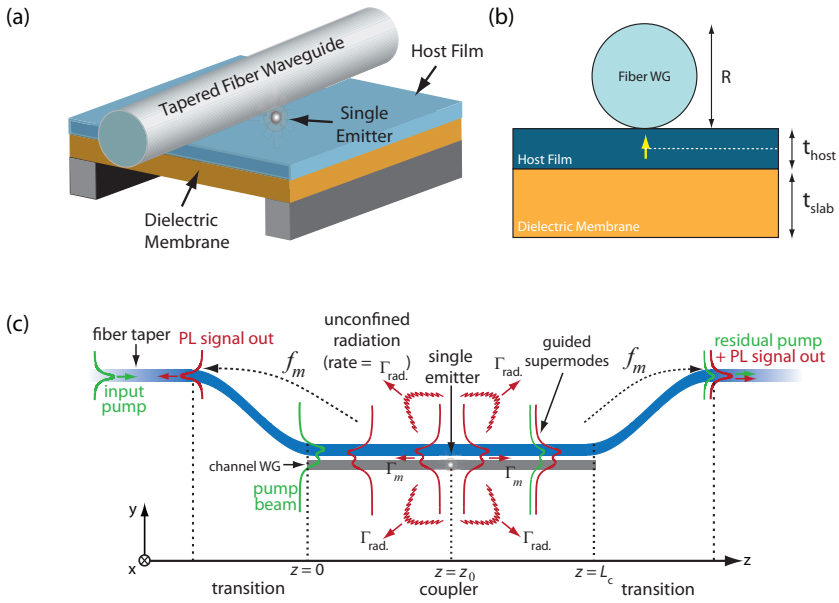

Fig. 1. (a) Tapered fiber waveguide-based probing configuration for emitters deposited on the surface of a dielectric membrane. An individual emitter, embedded in a host thin film, is depicted under the fiber. (b) Cross-section of structure in (a). (c) Schematic of single emitter excitation and PL collection via the tapered fiber probe. A non-resonant pump signal is injected into the input fiber and converted into a guided supermode of the composite waveguide, illuminating the slab-embedded dipole. The dipole radiates into guided and radiative supermodes, with rates Γ_m and Γ_{rad} respectively. Power is transferred with efficiency f_m from the supermode to the fiber mode and vice-versa. The interaction length L_c is the length in which fiber and slab are in close proximity.

ficiency.

The ability to perform spectroscopy of individual guest emitters in solid state hosts is desirable not only from a materials science perspective, in which the microscopic properties of either the host or the composite are investigated [5], but also for experiments in quantum optics, in which the control and manipulation of the quantum states of individual guest emitters is sought [6, 7]. Essential for both single emitter spectroscopy and quantum state manipulation is the availability of highly efficient access channels to the dipole, which, our previous work suggests [8, 9, 10], can be provided by an optical fiber taper waveguide.

The optical fiber taper waveguide is a single mode optical fiber whose diameter is adiabatically and symmetrically reduced to a wavelength-scale minimum, resulting in a low-loss, double-ended device with standard fiber input and output. The manner in which emitters on the surface of a dielectric mem-

brane may be optically accessed through the fiber is shown in Figs. 1(a)-(c). The wavelength-scale single mode region of the optical fiber waveguide is brought into proximity with the top surface of the membrane, over a length of several wavelengths. Fiber and membrane together form the composite dielectric waveguide with cross-section shown in Fig. 1(b), which supports a complete set of guided, leaky, and radiation supermodes originating from the hybridization of fiber and slab modes [11] (note that gap modes are indeed supermodes of the hybrid fiber-slab waveguide, as discussed in Section 4). As illustrated in Fig. 1(c), for non-resonant photoluminescence (PL) spectroscopy measurements, part of the non-resonant pump power initially carried by the fiber is coupled to supermode waves that reach the emitter. Illuminated by the pump, the emitter radiates (at a red-shifted wavelength) into supermodes of the composite waveguide, and a portion of the radiated power is outcoupled through the two fiber ends. Using the same method, we also envision the possibility of resonantly exciting the dipole, in which case the radiated fields (resonance fluorescence) would be coherent and at the same wavelength as the pump signal. Backward-propagating resonance fluorescence can potentially be collected from the input fiber port by way of a directional coupler. In the forward direction, the power at the output fiber is given by the interference between the excitation and resonant fluorescence signals, and may result in an enhanced or diminished transmission level [10, 12].

In [9], we analyzed the collection efficiency of the fiber taper waveguide for light emitted by a dipole embedded in a high refractive index membrane. We showed that the collection efficiency, achieved by tapping into emitted slab-confined waves, is potentially highly superior to that attainable with standard free-space collection using high numerical aperture optics. While the existence of the aforementioned gap modes was mentioned in that article, their potential application in performing efficient spectroscopy of individual surface-bound dipoles was only briefly discussed, and not analyzed at any level of detail. Such an analysis is accomplished in the following sections.

This paper is organized as follows. In Section 2, our simulation model and methods are explained. In Section 3, simulation results of fluorescence collection for two configurations appropriate for visible and infrared wavelengths are given. Section 4 analyzes the collection efficiency results in terms of a hybrid waveguide mode decomposition. Parameters from this analysis are used in Section 5 to show the possibility of resonant field extinction by a single dipole. A discussion of the results follows in Section 6, and Section 7 concludes the paper.

2. Model and methods

We envision a general spectroscopy configuration for probing individual emitters in highly dilute guest-host material systems, examples of which are: colloidal quantum dots (CdSe, CdSe/ZnO, PbS, PbSe, etc) in polymer [13] or sol-gel [14] hosts; organic dyes in polymer [15] or small-molecule crystalline hosts [6, 16, 17]; rare-earth ions in transparent solid-state hosts[18]. In our configuration, a thin film of the guest-host material system would be produced on top of a dielectric, high refractive index material, chosen appropriately according to the guest emitter transition wavelength ranges. For instance, a Si ($n \approx 3.5$) membrane could be used for near-infrared wavelengths above 1 μm, while SiN_x ($n \approx 2.0$) could be used for visible light emission. We point out that such thin-film structures may be produced in most cases with well-known, standard nanofabrication techniques. As depicted in Figs.1(a) and (b), a tapered optical fiber waveguide brought into contact with the host material provides both the excitation and collection channels to the guest emitters. We analyze this structure with the same method as in [9], where single emitter collection efficiency from dipoles embedded in a dielectric membrane was studied. The simulation model and analysis methods are briefly described below.

2.1. Simulation model

We model the problem as in Fig.1(b). An individual electric point dipole embedded in a thin host film on the surface of a dielectric membrane of thickness t_{slab} and refractive index n_{slab} is probed by an optical fiber taper waveguide of radius R and index $n_{\text{fiber}} = 1.45$. The dipole, oriented normal to the membrane surface, is assumed to be at the center of a dielectric host film of index n_{host} and thickness t_{host}. It is also assumed to be aligned with the center of the probing fiber. As in Fig. 1(c), an excitation signal, resonant or non-resonant with one of the emitter's transitions, is launched into the fiber input and adiabatically reduced in size as the fiber is tapered, exciting supermodes of the coupler structure. Supermodes with sufficient lateral confinement illuminate the dipole, at a position $z = z_0$ along the coupler. Under non-resonant excitation, the dipole emits coupler supermodes in the $\pm z$ directions, at a red-shifted wavelength. The emitted supermodes are converted into input and output fiber modes through the taper transition regions, after which emission is detected.

2.2. Fluorescence collection simulation

To estimate the PL collection efficiency of our fiber-based probing scheme, we simulated a single classical electric dipole radiating in the composite dielectric waveguide of Fig. 1(a), using the Finite Difference Time Domain (FDTD) method [9]. The simulation provided the steady-state fields over the entire com-

putational window, which was cubic, with more than six wavelengths in size. These were used to calculate an upper bound for the percentage of the total emitted power $P_{\text{Tot.}}$ coupled to the fundamental optical fiber mode at an arbitrary position z along the guide, with the expression

$$\eta_{\text{PL}} = 2\frac{P_z}{P_{\text{Tot.}}} f_{\text{fiber}}. \tag{1}$$

Here, P_z is the power flowing normally through the constant-z plane, f_{fiber} is the overlap integral in Eq. 2, taken between the radiated field at position z and the fundamental (isolated) fiber mode. The factor of 2 accounts for collection from both fiber ends. The symmetry of the geometry allowed us to choose symmetric ($\hat{\mathbf{x}} \times \mathbf{H} = 0$) boundary conditions on the yz-plane, as only y-polarized dipoles were considered. Perfectly-matched layers (PMLs) were used around the domain limits to simulate an open domain. Simulations ran until no field amplitude could be detected in the domain. As in [9], η_{PL} oscillates with z, due to the back-and-forth power exchange between the guide and the slab along the waveguide. The values of η_{PL} reported below correspond to maxima obtained within the computational window.

2.3. Supermode analysis

We analyze the results from the FDTD simulations in terms of the supermodes supported by the coupler structure formed by the fiber and slab. This provides us with insight into the collection mechanisms and ways to improve it, as well as the ability to determine the possibility of observing extinction of resonant input signals by a single dipole. The formalism we employ closely follows that used in our previous work [9].

Supermode field profiles and the respective complex propagation constants β_m are obtained with a finite-element based eigenvalue solver, with a vectorial formulation. Supermode m's individual contribution to the total PL collection efficiency η_{PL}, considering one fiber channel, is $\eta_{\text{PL},m} = f_m \cdot \Gamma_m/\Gamma = f_m \cdot \gamma_m$, where Γ_m is the supermode emission rate, and Γ the total emission rate. The fraction γ_m is supermode m's spontaneous emission coupling factor (β-factor), which, since emission in both $\pm z$ directions is equally likely, is such that $0 \leq \gamma_m \leq 0.5$. The fiber mode fraction, f_m, is the percentage of supermode m's power that is transferred to the output fiber mode. Assuming that the fiber is abruptly removed from the slab at the end of the probing region, and that reflections at the interface are small, f_m may be approximated with an overlap integral between the fundamental fiber mode and supermode m [19, 20]:

$$f_m = \frac{\text{Re}\left\{\iint_S (\mathbf{e}_f \times \mathbf{h}_m^*) \cdot \hat{\mathbf{z}}\, dS \iint_S (\mathbf{e}_m \times \mathbf{h}_f^*) \cdot \hat{\mathbf{z}}\, dS\right\}}{\text{Re}\left\{\iint_S (\mathbf{e}_f \times \mathbf{h}_f^*) \cdot \hat{\mathbf{z}}\, dS\right\} \text{Re}\left\{\iint_S (\mathbf{e}_m \times \mathbf{h}_m^*) \cdot \hat{\mathbf{z}}\, dS\right\}}. \tag{2}$$

In this expression, valid for purely dielectric waveguides, $\{\mathbf{e}_m, \mathbf{h}_m\}$ and $\{\mathbf{e}_f, \mathbf{h}_f\}$ are the supermode and fundamental fiber mode fields, respectively. The supermode emission rates Γ_m is also obtained from the field profiles, according to the expressions given in [9].

We point out that most of the supermodes supported by the fiber and membrane structure are leaky [11], i.e., power confined in the area beneath the fiber leaks away from it as the supermode propagates. The power leakage rate per propagation length is related to the imaginary part of the calculated supermode's complex effective index n_{eff}. The number of free-space wavelengths necessary for the supermode amplitude to decay by a factor $0 < \delta < 1$ is $N_\delta = -n_i^{-1} \ln(\delta)/2\pi$, where $n_i^{-1} = \mathrm{Im}\{n_{\mathrm{eff}}\}^{-1}$, and an effective supermode propagation length $L_{\mathrm{eff},\delta} = N_\delta \lambda$ may be defined.

2.4. Field Extinction

For coherent, resonant excitation, the power detected at the output fiber port is a result of the interference between the excitation signal and the resonance fluorescence from the emitter (which are at the same wavelength), and may be either higher or lower than the detected power in the absence of the dipole. In order to determine the variation in the transmitted power level due to the presence of a single dipole, we make use of the quantum optics input-output formalism of [21], with which we obtain operators for the multimode field for $z > z_0$, i.e., past the dipole location:

$$\mathbf{E}^{(+)}(z,t) = i\sqrt{2\pi} \sum_m \sqrt{\frac{\hbar\omega}{4\pi S_m}} \mathbf{e}_m e^{-i(\omega t - \beta_m z)} \times \\ \times \left[\hat{a}_{in}^m (t - n_m z/c) + \sqrt{\Gamma_m}^* \sigma_-(t - n_m z/c) \right]. \quad (3)$$

Here, σ_- is the atomic lowering operator, $\hat{a}_{in}^m$ is (incident) supermode m's input field annihilation operator, $\mathbf{e}_m$ is the electric field distribution, β_m the propagation constant, n_m the phase index, and $S_m = \mathrm{Re}\{\int_S dS(\mathbf{e}_m \times \mathbf{h}_m^*) \cdot \hat{\mathbf{z}}\}$, with S the xy plane. The expression in brackets is a well-known result of the input-output formalism, with explicit input (or "free") fields and radiated ("source") contributions [21], expanded in terms of supermodes. The field operators are then inserted in the fiber mode power operator [10],

$$\hat{F} = \left\{ \int_S dS(\mathbf{E}^{(-)} \times \mathbf{h}_f) \cdot \hat{\mathbf{z}} \int_S dS(\mathbf{e}_f^* \times \mathbf{H}^{(+)}) \cdot \hat{\mathbf{z}} + \right. \\ \left. \int_S dS(\mathbf{H}^{(-)} \times \mathbf{e}_f) \cdot \hat{\mathbf{z}} \int_S dS(\mathbf{h}_f^* \times \mathbf{E}^{(+)}) \cdot \hat{\mathbf{z}} \right\} S_f^{-1}, \quad (4)$$

where $\mathbf{e}_f$ and $\mathbf{h}_f$ are the fiber mode electric and magnetic field distributions, $S_f = \mathrm{Re}\{\int_S dS(\mathbf{e}_f \times \mathbf{h}_f^*) \cdot \hat{\mathbf{z}}\}$. In short, the fiber mode power operator allows us

to determine the total photon flux coupled into the output fiber mode, based on multimode field operators that describe the coherent interference between the incident ('free') and emitted, resonance fluorescence ('source') supermode waves; the operator is the quantum optics equivalent to the overlap integral in Eq. (2), between the total field at a position z along the waveguide and the optical fiber mode. This corresponds to the power coupled into the output fiber at the end of the coupling region, assuming an abrupt transition and small reflections at the interface [19]. Considering coherent, steady-state, multimode field excitation, the photon flux F at the output fiber (normalized to the input field power) is found to be

$$\begin{aligned} F &= \hbar\omega \mathrm{Re}\left\{ \sum_{m,m'} \sqrt{f_m}\sqrt{f_{m'}} e^{i(\beta_{m'}-\beta_m)(z-z_0)} \times \right. \\ &\times \left. \left[B_m B_{m'}^* + \frac{\sqrt{\Gamma_m}\sqrt{\Gamma_{m'}}^* \zeta - \frac{\Gamma}{2}\left(B_m^* \sqrt{\Gamma_{m'}}^* \xi + B_{m'}\sqrt{\Gamma_m}\xi^* \right)}{\left(\frac{\Gamma}{2}\right)^2 + 2\zeta} \right] \right\}, \end{aligned} \tag{5}$$

with $\xi = \sum_m \sqrt{\Gamma_m} B_m$, $\zeta = \sum_{m,m'} \mathrm{Re}\left\{ \sqrt{\Gamma_m}\sqrt{\Gamma_{m'}}^* B_m^* B_{m'} \right\}$. In this expression, B_m is the complex amplitude of the m-th supermode incident on the dipole. The magnitude of B_m is determined by the manner with which the fiber is brought into contact with the slab. For instance, for abrupt contact (e.g., very short transition regions in Fig.1), it approaches $|f_m|^{1/2}$, where f_m is the fiber-mode fraction. Longer transition regions could lead to a power distribution among the excited supermodes different from that obtained with the fiber-mode fractions. The phase of the B_m coefficients at the dipole position is determined through the supermode propagation constants β_m, assuming all modes are in-phase at the start of the coupler region.

To gain some insight into the mechanisms at play at resonant excitation, we consider a situation in which only one supermode of the fiber and slab structure may be accessed: in Eq.(5), we set all fiber-mode fractions f_m and incident supermode amplitudes B_m to be null except for those of an arbitrary M-th supermode (i.e., $f_{m\neq M} = 0$, $B_{m\neq M} = 0$). We furthermore make the assumption that the excitation signal drives the transition far from saturation, so that $\zeta/\Gamma^2 \ll 1$ and the denominator of the second term in brackets becomes unity. In this case, the power detected at the output fiber is proportional to $1 - 4\gamma_M(1-\gamma_M)$. Thus the magnitude of optical field extinction by a single dipole is determined by the supermode spontaneous emission coupling factor, and is complete when $\gamma_M = 0.5$.

3. Fluorescence Collection Efficiency

Two configurations were analyzed, for operation at visible ($\lambda = 600$ nm) and near-infrared ($\lambda = 1300$ nm) wavelengths. For the visible range, a 130 nm thick SiN membrane (refractive index n_{SiN} = 2.0) and 400 nm diameter single mode fiber taper waveguide were considered. In the near-infrared case, our model consists of a 160 nm thick Si membrane (refractive index n_{Si} = 3.505) and a 1 μm diameter fiber taper, which supports a well-confined and a near-cutoff mode. The first configuration models a system suitable for probing visible wavelength emitters such as single molecules or CdTe/ZnSe nanocrystal quantum dots attached to the SiN membrane, while the second would be suitable for infrared emitters, such as PbS and PbSe nanocrystal quantum dots [22]. In both cases, the emitters are considered to be embedded in a 20 nm thick, purely dielectric host film on top of the SiN or Si membranes, as shown in Fig.1(b). The host film refractive index n_{host} is allowed to vary between 1.0 and 1.7, a range that includes typical values for possible organic (e.g., PMMA) or inorganic (e.g., silica) transparent host materials. The emitters are modeled as electric dipoles oriented in the *y*-direction. While this consideration limits our analysis to a best-case scenario for emitters with random dipole orientation, it may be well suited to model certain organic crystal guest-host systems, where emitting molecules embedded in the host crystal tend to align in specific orientations. For instance, in the guest-host system presented in [23], consisting of Terrylene molecules in a crystalline *p*-terphenyl host -a system fit for molecular quantum optics [6]-, the guest molecules have been shown to display dipole moments perpendicularly oriented to the substrate.

Figure 2(a) shows the FDTD-calculated total spontaneous emission rate Γ, for a *y*-polarized dipole in the SiN ($\lambda = 600$ nm) and Si ($\lambda = 1300$ nm) membrane configurations, as functions of the host layer refractive index, n_{host}. All rates are normalized to the rate for a dipole in a homogeneous space of index n_{host} ($\Gamma_{\mathrm{Hom.}}$) and thus correspond to the spontaneous emission enhancement (Purcell) factor. Purcell factors as high as 20 and 9 respectively are observed for $n_{\mathrm{host}} = 1.0$ in the Si and SiN cases, and decrease with increasing host index. Simulations with progressively denser meshes were used to verify that these results converged to within at least 3 %.

In Fig. 2(b), the corresponding maximum PL collection efficiencies η_{PL} including collection from both fiber ends are plotted. As mentioned earlier, since η_{PL} oscillates in z due to power exchange between the fiber and slab, the plotted values correspond to the maximum efficiency within the computational window (with dimensions > 6 wavelengths). It is apparent that collection efficiencies are above 18 % for all n_{host} in both Si and SiN cases, with maxima of 22.8 % and 20.5 % at $n_{\mathrm{host}} = 1.0$ respectively, and decreasing for higher values.

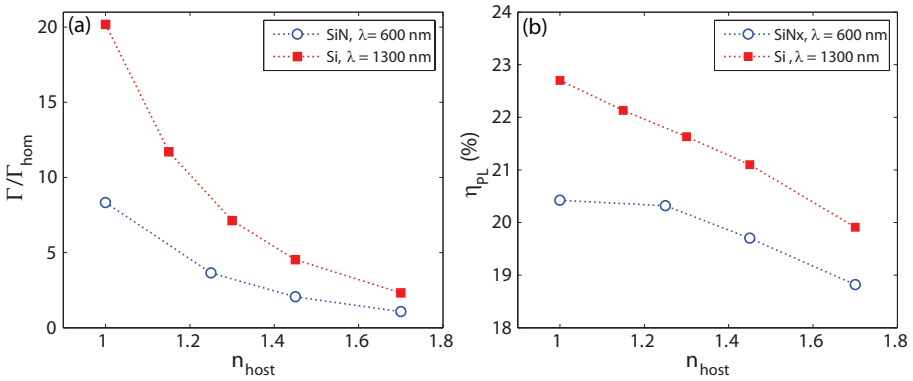

Fig. 2. (a)Maximum total spontaneous emission rate enhacement $\Gamma/\Gamma_{\mathrm{hom}}$, where Γ_{hom} is the spontaneous emission rate of a dipole in a homogeneous dielectric medium of refractive index n_{host}. (b) PL collection efficiencies η_{PL}, including both fiber ends, for y-polarized dipoles in the SiN ($\lambda = 600$ nm) and Si ($\lambda = 1300$ nm) membrane configurations, as functions of the host layer refractive index, n_{host}. Results calculated with finite difference time domain simulations.

4. Supermode Analysis

A modal analysis of the the coupler structures formed by the fiber and membranes (cross section shown in Fig.1(b)) reveals the existence of laterally confined supermodes, such as depicted in Figs. 3(a) and (c), with a predominantly y-polarized electric field strongly concentrated in the host material layer. The strong field concentration translates into an enhanced dipole coupling strength, and leads to the spontaneous emission enhancement reported in Section 3. Group velocities are not significantly low, so the density of modes does not play an important role in emission enhancement, contrasting with the situation in slow-light photonic crystal waveguides [24, 25].

In both, Si and SiN, systems, the strong field concentration originates in the large index steps between the membrane and host layer. Such gap modes are the main contributors to the total collection efficiency, η_{PL}. This is apparent in Figs. 4 (a) and (e), where the individual contributions, $\eta_{\mathrm{PL,m}}$, to the total collection efficiency, η_{PL}, are plotted. The contributions of all secondary supermodes (black dots in Fig.4 (a) and (e)) are at least an order of magnitude smaller than the main ones. Despite providing small individual contributions, secondary supermodes altogether make up for a large portion of the total collected power. It is important to note that, even though many of the secondary supermodes are indeed gap modes, poor lateral confinement causes these to exhibit large effective areas, and therefore low emission rates Γ_m. Correspondingly, low emission coupling factors γ_m ($\gamma_m = \Gamma_m/\Gamma$, with Γ the total spontaneous emission rate)

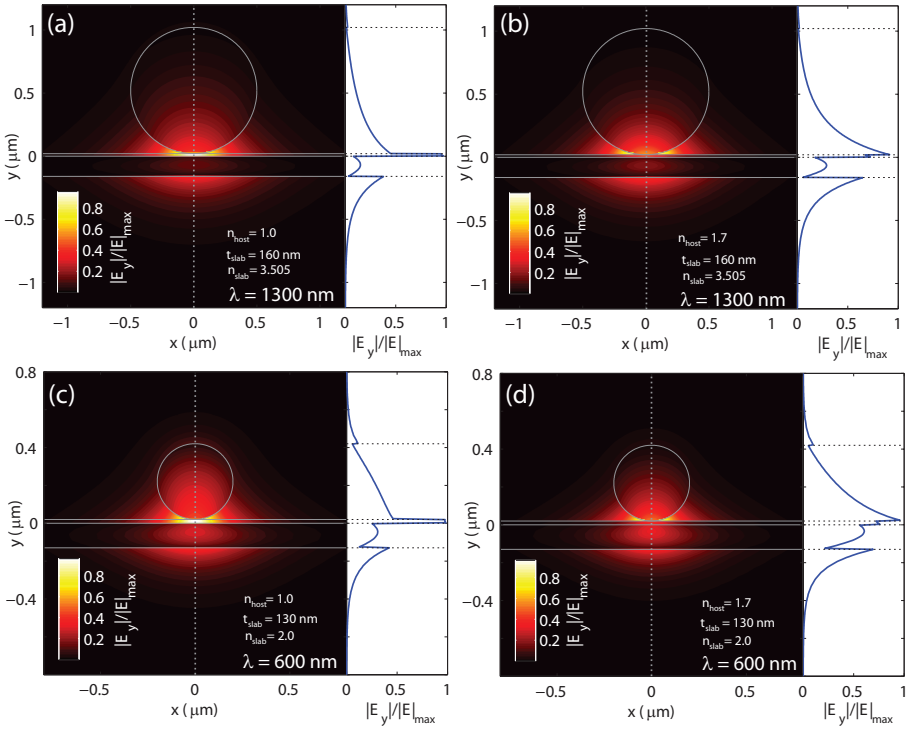

Fig. 3. Amplitude of the major electric field component (E_y) of laterally bound gap modes (normalized to the maximum electric field amplitude, $|\mathbf{E}|_{\max}$) for the (a)-(b) Si slab configuration ($\lambda = 1300$ nm) with (a) $n_{\text{host}} = 1.0$ and (b) $n_{\text{host}} = 1.7$; (c)-(d) SiN configuration ($\lambda = 600$ nm) with (c) $n_{\text{host}} = 1.0$ and (d) $n_{\text{host}} = 1.7$. In all cases, t_{host} = 20 nm. Line plots show $|E_y|/|\mathbf{E}|_{\max}$ on the $x = 0$ plane (dotted line in the contour plots).

are observed in Figs. 4(b) and (f). For the main modes, $\gamma_m > 10$ %, so these gap modes carry a considerable percentage of the total spontaneous emission.

The oscillation of the total efficiency η_{PL} as a function of z, mentioned in Section 3, can be traced to the beating of the two main contributing supermodes. The beat length is given by $L_z = 2\pi/(\Delta\beta)$, where $\Delta\beta$ is the difference between the propagation constants. For the Si, $\lambda = 1.3$ μm configuration, the beat length varies between 4.78 μm, for $n_{\text{host}} = 1.0$ and 3.89 μm, for $n_{\text{host}} = 1.7$. In the SiN, $\lambda = 0.6$ μm case, it varies between 2.72 μm, for $n_{\text{host}} = 1.0$ and 2.17 μm, for $n_{\text{host}} = 1.7$. In order to maximize the collected power, therefore, control of the interaction length L_c on the scale a few microns is desirable.

At the same time, short interaction lengths L_c are desirable because all supermodes exhibit some degree of lateral power leakage due to imperfect field confinement. Figures 4(d) and (h) show the effective lengths $L_{\text{eff},\delta}$, defined in Section 2.3, necessary for 10 % supermode amplitude decay, for the Si and SiN

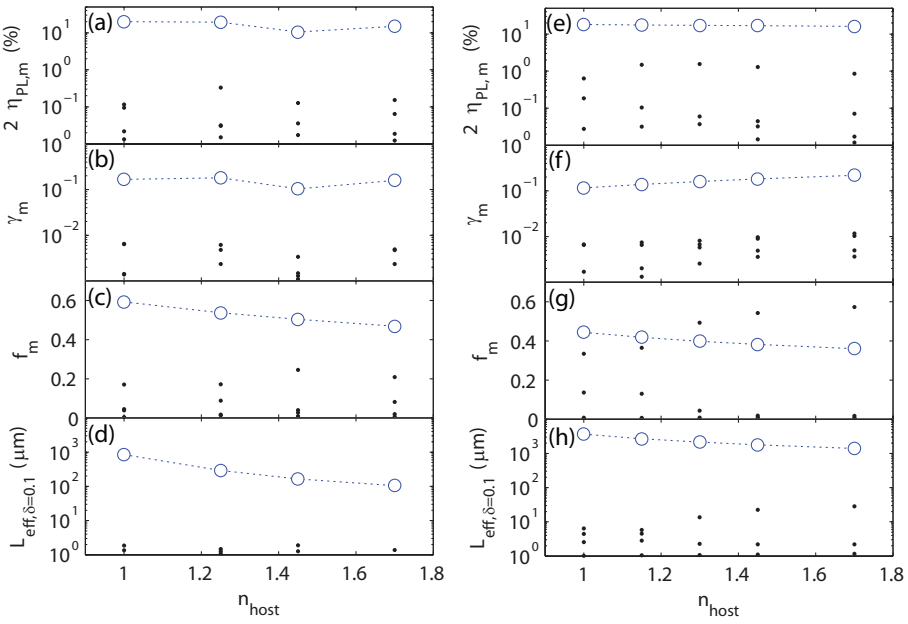

Fig. 4. Supermode contributions to the total PL collection efficiency ($\eta_{\mathrm{PL,m}}$), modal spontaneous emission coupling factors (γ_m), fiber mode fractions f_m and effective supermode lengths $L_{\mathrm{eff},\delta=0.1}$ for the (a)-(d) Si slab, $\lambda = 1300$ nm and (e)-(h) SiN, $\lambda = 600$ nm systems. Circles: main supermode; dots: secondary supermodes

case respectively. It is apparent that in both cases the main supermodes have considerably longer (more than two decades) effective lengths, as expected, in view of their lower lateral power leakage rate. For the Si structure at $\lambda = 1300$ nm, the necessary length for the main supermode to decay by 10 % varies between 3650 μm and 1400 μm for the host index range considered. In the SiN case at $\lambda = 600$ nm, the 10 % decay length ranges between 1840 μm and 225 μm. For interaction lengths L_{c} of only a few microns, the main supermode contributions in Figs. 4 (a) and (e) may thus be taken as lower bounds for the total achievable collection efficiency.

5. Resonant Extinction Spectroscopy

The SiN membrane configuration offers positive prospects for performing extinction-based single emitter spectroscopy measurements with a coherent resonant excitation signal [12]. The main contributing supermode has a modal spontaneous emission coupling factor $\gamma_m > 0.1$ with maximum of 0.18 for n_{host}=1.25 (see Fig. 4(f)); if excited alone, the field extinction at the output fiber could be higher than 37 %, with a maximum of 60 % for $n_{\mathrm{host}} = 1.25$. For an abrupt transition, however, as explained above, additional supermodes would be

excited, with efficiencies given by the fiber-mode fractions f_m. Such additional supermodes are not strongly extinguished by the dipole, having $\gamma_m < 0.006$, and thus limit the achievable overall extinction at the output fiber. To estimate output fiber power extinction, we use Eq. (5) with the three highest contributing supermodes, considering $n_{\text{host}} = 1.7$. The percentage of fiber mode power carried by these three supermodes altogether amounts to 75.5 % (see Fig. 4(g)). We assume that the remainder of the power is completely transferred to the output fiber, a worst-case scenario which implicitly assumes that none of this power leaks away from the fiber, or is reflected by the dipole. Figure 5 (a) shows the calculated optical flux at the output fiber for light on- and off-resonance (F and F_0) with a y-oriented dipole in a host material of index 1.7, as well as the transmission contrast through the fiber, $\Delta T = (F - F_0)/F_0$. In the figure, the horizontal axis is the distance from the dipole to the end of the coupler region, as indicated in Fig. 1, and $z_0 = 1$ μm. The oscillations in F, F_0 and ΔT along z evidence the back-and-forth power transfer between fiber and slab, and the amplitude decay is indicative of both the interference and leaky nature of the supermodes involved. It is apparent that, for $z - z_0 \gg 0$, the extinction level may reach ≈ 20 %.

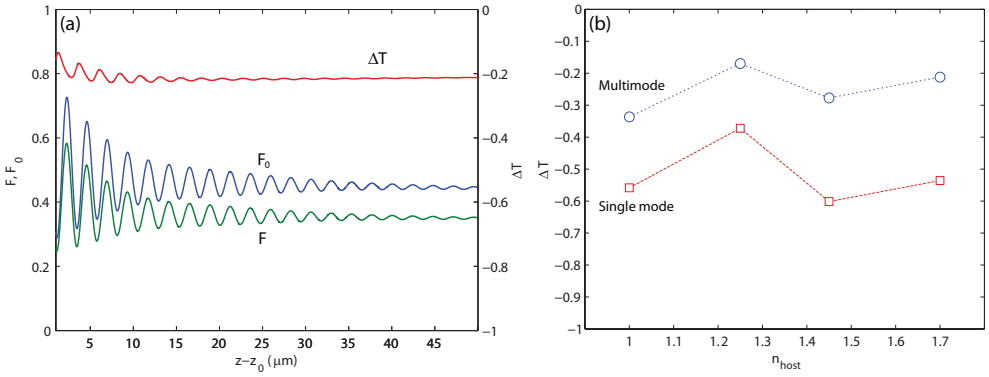

Fig. 5. (a) Normalized, off- and on-resonance transmission (F_0 and F) and contrast $\Delta T = (F - F_0)/F_0$ as functions of separation from a single, y-oriented dipole at z_0. The dipole is embedded in a host material with $n_{\text{host}} = 1.7$ on top of a 130 nm thick SiN membrane, and emits at $\lambda = 600$ nm. (b) Achievable transmission contrast ΔT as a function of the host film index n_{host}. Squares: results obtained assuming dipole excitation with the main supermode only; circles: assuming multimode excitation (see text for details).

Figure 5(b) shows the achievable extinction ratio at $z - z_0 = 50$ μm, under the same assumptions, for all host indices considered (circles). We also plot the extinction levels achievable under the single supermode assumption (squares), which makes explicit the degradation of extinction due to the excitation of ad-

ditional supermode waves. The highest achievable extinction may be as much as 34 % for $n_{\text{host}} = 1.0$, for which the Purcell enhancement is maximum and considerably stronger than for $n_{\text{host}} = 1.7$. This result suggests that, as long as the input signal power is sufficiently below the transition saturation power, the Purcell effect does not influence the achievable extinction level. This is to be expected, given that the aforementioned expression for extinction in the case of single mode excitation and collection, $F \sim 1 - 4\gamma_m(1 - \gamma_m)$, only depends on the modal spontaneous coupling factor γ_m. Purcell enhancement will influence the power at which dipole saturation occurs, and may thus have implications in obtaining better detection signal-to-noise ratios.

Similar performance may in principle be achieved with the Si system, for an appropriate set of parameters. The situation, however, is less favorable for the parameters considered here: in Fig. 4(c), for $n_{\text{host}} > 1.2$, the main supermode fiber fraction is surpassed by that of the second mode, which is only weakly affected by the dipole ($\gamma_m < 0.01$ in Fig. 4(b)). Assuming that the second supermode is completely transmitted, that 40 % of the power in the fiber is carried by the main supermode (see Fig. 4(c)), and that the latter is extinguished by 31 % ($\gamma_m = 0.22$, Fig. 4(b)), the maximum achievable overall extinction would be only 12 %. Although lower than in the SiN cases studied above, such an extinction level is still quite reasonable for spectroscopy purposes, and is compatible with experimentally observed levels using an NSOM tip [12] and a solid immersion lens [26].

6. Discussion

In slot waveguides consisting of two high refractive index channels separated by a small gap [1], strong field concentration in the gap results from the continuity of the normal electric displacement vector component at dielectric interfaces, with the field concentration increasing for increasing refractive index discontinuity. This behavior is evident in Figs. 3(a),(b) and (c),(d), which depict the intensity of the electric field in the host region, for host film refractive indices $n_{\text{host}} = 1.0$ and $n_{\text{host}} = 1.7$, for both the Si and SiN configurations. The decrease in field concentration for larger indices is apparent in the Purcell factor decrease for increasing host material index n_{host} (Fig. 2(b)). However, even in situations where the Purcell factor is small, gap supermodes have relatively high modal spontaneous emission coupling factors (γ_m) and efficient coupling to the fiber mode (f_m) (see Fig. 4), which creates the conditions for performing extinction-type, resonant spectroscopy on individual emitters.

We point out that the cases in which the highest Purcell enhancements are observed, in which $n_{\text{host}} = 1.0$, would be challenging or not achievable in practice. These situations, which otherwise provide upper bounds for the achievable enhancement, imply the absence of a host material supporting the emitter, or, in

the best case, the ability to produce a 20 nm thick host layer of extremely low refractive index material, for instance an aerogel. It is also worthwhile noting that, although semiconductor nanocrystal quantum dots are composed of high refractive index materials, sufficiently small nanocrystals may not constitute a significant disturbance to the environment, that could lead to large deviations from our calculated results. Evidence of this can be found in [27], where small (< 5 nm) PbS nanocrystal quantum dots were shown to not considerably affect the modes of a high quality factor microresonator. A similar conclusion may be drawn from the simulations involving diamond nanocrystals in nanocavities reported in [28].

We reiterate that the results presented here are best-case estimates, obtained for vertical dipole moments aligned with the gap mode field. Horizontal dipole moments are expected to radiate at lower rates. In the case of z-dipoles, gap waves are generated at lower rates because the dipole moment is aligned with the minor supermode field component, E_z. If located at the $x = 0$ plane, an x-dipole is completely uncoupled from gap modes, producing, rather, anti-symmetric ($\hat{\mathbf{y}} \times \mathbf{E}|_{x=0}$=0) supermode waves with a major x-field component. These do not offer the same strong field concentration as gap modes, due to the continuity of the electric field across the gap.

As in the situation studied in [9], relating to PL collection from slab-embedded dipoles, lateral modal confinement plays an important role. Despite the high γ_m factors of the main gap supermodes, a significant portion of the dipole power is emitted into supermodes with very poor lateral confinement, which in a short distance along z propagate away from the fiber and are not collected. Thus, the length of the interaction region must be minimized for a maximized collection. In addition, enforcing strong lateral confinement via the formation of a channel, rather than a membrane, may significantly enhance collection efficiency. For instance, by replacing the SiN membrane studied above with a channel waveguide of the same thickness, but with a width of 600 nm and with a host material of index $n_{\text{host}} = 1.45$, a collection efficiency of ≈ 49 % may be achieved with a Purcell factor of ≈ 2. Additionally, as in [10], a channel waveguide structure may also benefit resonant excitation experiments, not only with an enhanced resonance fluorescence collection efficiency, but also with higher extinction levels, or even enhancement of the output power relative to the transmission level without the dipole. In this case, tapered fiber and channel waveguides may be designed to form a phase-matched directional coupler, with high γ_m supermodes. The waveguide could furthermore be designed to allow efficient power transfer from the fiber to a single supermode, so that the single-mode situation mentioned in Section 5 may be achieved. In this case, provided the single supermode's γ_m is large, high field extinction may be achieved independent of the coupler length or emitter position along its length [10]. For

the channel waveguide situation just described, $\gamma_m = 0.215$ for the main supermode, which would lead to a single-mode extinction of 67 %.

Finally, we point out that the recently reported plasmonic laser [29], composed of a cylindrical CdS nanowire placed on top of a Ag substrate, with a thin MgS separator (the cross section closely resembles that in Fig. 1(b)) supports gap modes similar to those studied here. While here the supermodes are hybrids of fiber and slab modes, those in [29] are hybrids of the cylinder and surface plasmon modes. Although hybrid plasmonic waveguides offer substantially stronger Purcell enhancement for emitters located in the MgS spacer or in the nanowire, the supermodes suffer from high propagation losses associated with the surface plasmon. Indeed, supermode propagation lengths (i.e., the required length for the mode power to drop in half) quoted in [29] are on the order of 10 wavelengths. In the present case, supermode effective lengths are two to three orders of magnitude longer, since the waveguides are purely dielectric, and lateral power leakage is small.

7. Conclusions

We have performed detailed electromagnetic simulations that indicate that a tapered optical fiber waveguide may be an efficient photoluminescence collection probe for individual dipoles placed on the surface of dielectric membranes. High maximum collection efficiencies (> 20 %) are predicted, and are related to hybrid supermodes of the composite fiber-slab structure, which present strong field concentration in the gap between slab and fiber. These supermodes are akin to the gap modes supported by slotted waveguides [1]. Our results also indicate that this probing configuration may be used to perform resonant spectroscopy of single emitters on membrane surfaces, and we predict that an extinction of at least 20 % of a fiber-coupled resonant excitation signal is achievable.

Acknowledgement

This work has been supported in part by the NIST-CNST/UMD-NanoCenter Cooperative Agreement.